ELSEVIER

Ceramics International 32 (2006) 385–392

CERAMICS INTERNATIONAL

www.elsevier.com/locate/ceramint

The role of counterions (Mo, Nb, Sb, W) in Cr-, Mn-, Ni- and V-doped rutile ceramic pigments Part 1. Crystal structure and phase transformations

F. Matteucci [a,*], G. Cruciani [b], M. Dondi [a], M. Raimondo [a]

[a] *Institute of Science and Technology for Ceramics (ISTEC), Via Granarolo 64, 48018 Faenza, Italy*
[b] *Earth Science Department, University of Ferrara, Corso Ercole I d'Este 32, 44100 Ferrara, Italy*

Received 17 January 2005; received in revised form 18 February 2005; accepted 20 March 2005
Available online 31 August 2005

Abstract

Rutile is widely used as ceramic pigment for its excellent optical properties, high melting point and intense coloration when doped with transition elements. Industrial ceramic pigments are manufactured from anatase plus chromophore elements (Cr, Mn, Ni or V) and counterions (Nb, Sb or W). Several solid state reactions occur during the synthesis, involving both the anatase-to-rutile transformation (A → R) and the formation of accessory phases. The A → R transition is heavily affected by chromophores with a lowering of the onset temperature: V < Cr < Ni < Mn; the effect of counterions is almost completely hidden by that of chromophores, even if the sequence Mo < Sb < W < Nb may be inferred. The crystal structure of rutile pigments is modified by chromophores and counterions doping; in fact, the doping varies the cell parameters, implies a progressive distortion of the octahedral site and a peculiar variation of the mean Ti–O bond length, with longer basal Ti–O distances and a shorter apical Ti–O distance. The pigment co-doped with V and W is different for its minimum Ti–O bond length distortion (BLD), an almost regular TiO_6 octahedron, and the occurrence of Ti^{3+} within the accessory compound Ti_5O_9.

Keywords: B. X-ray methods; D. TiO_2; D. Traditional ceramics; Anatase-to-rutile transformation; Ceramic pigments

1. Introduction

The rutile structure is widely used as ceramic pigment for its excellent optical properties (refractive indices $N_O = 2.612$ and $N_E = 2.889$), high melting point (~1800 °C) and capacity to develop intense coloration when doped with chromophore elements [1–3].

The structure of rutile, space group $P4_2/mnm$, is constituted by chains of TiO_6 octahedra, sharing a vertex along the *c* axis, where practically every first row transition element – and even metals of further rows – can be hosted [3].

The pigments based on the rutile structure are characterised by the occurrence of both a chromophore element and a counterion with a valency ≥(IV), which is thought to balance the charge mismatch between Ti^{4+} and chromophore element (usually with (II) or (III) valency state) so ensuring the electroneutrality of the lattice [1–4].

Several industrial pigments are manufactured starting from anatase plus oxides of chromophore elements (Cr, Mn, Ni or V) and counterions (Nb, Sb or W) with addition of mineralisers [1–3]. Other elements are sometimes used in the industrial practice, even if not considered by the DCMA list [5], especially Mo as counterion [1].

The colour is achieved by calcination at temperatures around 1000 °C and its development seems to occur during the anatase-to-rutile transformation (hereafter A → R) [3,6]. Within the wide literature on this transition, several papers consider the elements used in rutile pigment manufacturing [7–15], but studies concerning the coupling of chromophore + counterion are limited to a few systems [16–20].

The approach of the present study consists in the preparation of the entire range of rutile-based industrial

* Corresponding author. Tel.: +39 0546 699738; fax: +39 0546 46381.
E-mail address: matteucci@istec.cnr.it (F. Matteucci).

0272-8842/$30.00
doi:10.1016/j.ceramint.2005.03.014

pigments, including all combinations of a chromophore (Cr, Mn, Ni and V) with a counterion (Mo, Nb, Sb and W), even though not present in the DCMA list. These pigments were then characterised by X-ray diffraction, following the evolution of the phase composition during the calcination process and appraising the effect of counterions on:

- the anatase-to-rutile transition;
- the transformations, involving phases of chromophore elements and counterions, which occur during the pigment synthesis;
- the structure of rutile, with special emphasis on those parameters which are expected to affect directly the pigment coloration (e.g. Ti–O bond distances, distortion of the octahedral site).

The second part of this study deals with the colouring and technological behaviour of rutile pigments, trying to point out the dependence of colour on crystal structure and occurrence of secondary phases.

2. Materials and methods

Sixteen compositions of ceramic pigments were prepared at the laboratory scale with stoichiometry $Ti_{1-2x}A_xB_xO_2$, where A = Cr, Mn, Ni or V; B = Mo, Nb, Sb or W; $x = 0.03$, plus a reference sample with $x = 0$. The samples are named by two letters: the first for the chromophore (C, M, N and V for Cr, Mn, Ni and V, respectively) and the second for the counterion (M, N, S and W for Mo, Nb, Sb and W, respectively); the undoped titania is referred to as AA.

The raw materials used are: anatase (Degussa DT51) and reagent-grade oxides of chromophores (Cr_2O_3, Mn_2O_3, NiO, V_2O_5) and counterions (MoO_3, Nb_2O_5, Sb_2O_3, WO_3). Any type of mineraliser was added.

The pigments were synthesised by the conventional ceramic process: wet mixing of raw materials in porcelain jar with alumina grinding media, drying in oven at 105 °C, then calcination in alumina crucibles in an electric kiln at five maximum temperatures: 700, 800, 900, 1000 and 1100 °C, with thermal rate of 200 °C/h, soaking time of 1 h and ''natural'' cooling to room temperature.

The calcined samples were ground in an agate mortar and sieved below 50 μm, then characterised by X-ray powder diffraction under different conditions:

- graphite-monochromated Cu $K\alpha_{1,2}$ radiation, 15–130°2θ range, scan rate 0.02°2θ, 10 s per step (Philips mod. 1820/00) for the samples synthesised at 1100 °C;
- Ni-filtered Cu Kα radiation, 10–60°2θ range, scan rate 0.04°2θ, 1 s per step (Rigaku mod. Miniflex) for the samples calcined between 700 and 1000 °C.

The structural refinements of samples calcined at 1100 °C were performed by the Rietveld method, using the GSAS-EXPGUI software [21,22]. Starting atomic parameters for the rutile were taken from Howard et al. [23] and then used on the whole series of refinements.

Depending upon the presence of impurities refined variables ranged up to 28 independent variables, including: scale-factors, zero-point, 6 ÷ 15 coefficients of the shifted Chebyschev function to fit the background, rutile cell dimensions, atomic positions, profile coefficients (one gaussian [GW] and two lorentzian terms [L_x,L_y]). Concerning isotropic displacement parameters, they were refined during the first cycles, but then fixed in the 0.6–1.4 U_{ISO} range depending on the refinement. The number of variables

Table 1
Rietveld refinement parameters (number of independent variables, figures-of-merit) and structural data of rutile pigments synthesised at 1100 °C

Sample	Variables	RF^2	wRp	Rp	Cell parameters			Oxygen position and isotropic displacement parameters		
					$a = b$ (Å)	c (Å)	V (Å^3)	U_{ISO} (Ti)	U_{ISO} (O)	x (O)
AA	21	0.046	0.192	0.156	4.5947 (1)	2.9593 (1)	62.47	1.2	0.9	0.3045 (1)
CM	23	0.066	0.200	0.163	4.5948 (2)	2.9586 (1)	62.46	0.8	0.8	0.3033 (1)
CN	19	0.047	0.163	0.134	4.5971 (1)	2.9622 (1)	62.60	0.8	0.7	0.3038 (1)
CS	23	0.047	0.162	0.128	4.5950 (1)	2.9648 (1)	62.60	1.1	1.4	0.3049 (1)
CW	18	0.053	0.195	0.156	4.5933 (2)	2.9583 (1)	62.41	0.8	0.7	0.3028 (1)
MM	27	0.053	0.182	0.147	4.5955 (1)	2.9582 (1)	62.48	0.8	0.7	0.3038 (1)
MN	24	0.053	0.175	0.140	4.5970 (1)	2.9603 (1)	62.56	0.8	0.7	0.3049 (1)
MS	25	0.055	0.159	0.129	4.5955 (1)	2.9623 (1)	62.56	0.8	0.7	0.3030 (1)
MW	23	0.036	0.176	0.140	4.5984 (1)	2.9575 (1)	62.54	1.2	1.6	0.3044 (1)
NM	24	0.069	0.218	0.178	4.5955 (2)	2.9585 (3)	62.48	0.8	0.7	0.3039 (1)
NN	25	0.043	0.160	0.128	4.5975 (1)	2.9621 (1)	62.61	1.2	1.1	0.3039 (1)
NS	17	0.038	0.173	0.137	4.5960 (1)	2.9645 (1)	62.62	1.1	1.3	0.3038 (2)
NW	20	0.046	0.164	0.132	4.5978 (1)	2.9597 (1)	62.57	0.8	0.7	0.3030 (1)
VM	15	0.067	0.228	0.178	4.5905 (1)	2.9564 (2)	62.30	0.7	0.6	0.3031 (1)
VN	21	0.043	0.208	0.161	4.5930 (1)	2.9607 (1)	62.46	1.0	0.8	0.3036 (1)
VS	18	0.040	0.174	0.141	4.5926 (1)	2.9630 (1)	62.50	1.0	1.2	0.3035 (1)
VW	26	0.066	0.216	0.170	4.5921 (1)	2.9583 (2)	62.38	0.8	0.7	0.3013 (1)

Note: values shown in parentheses are estimated standard deviations in last decimal figure. Each X-ray powder diffraction pattern consisted of 5750 data points and 78 independent observations. U_{ISO} are shown as $\times 10^2$ Å^2.

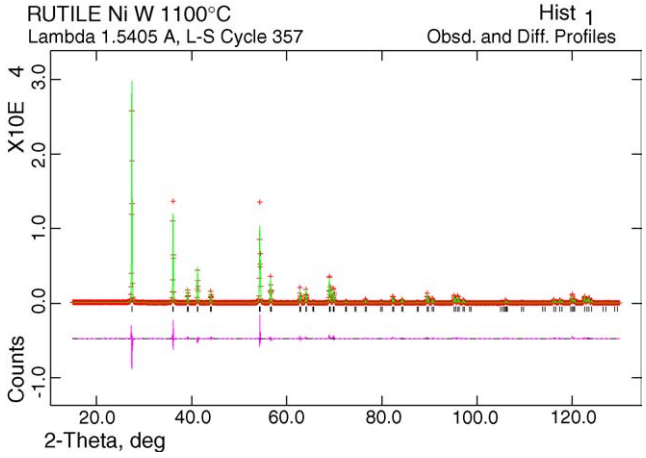

Fig. 1. Rietveld refinement plot of the X-ray powder diffraction data NW11. In the figure, the continuous lines represent calculated pattern, while cross points show the observed pattern. The difference curve between observed and calculated profiles is plotted below.

and observations as well as the figures-of-merit of every refinement are summarised in Table 1 and an example of a Rietveld refinement plot is showed in Fig. 1. The bond length distortion (BLD) was calculated as $BLD = 10 \times \Sigma_i(B–O_{av}–B–O_i)/B–O_{av}$, where $B–O_{av}$ is the average metal-ligand distance and $B–O_i$ is the ith metal–ligand distance.

The quantitative phase analysis was carried out using different methods. The Rietveld method was carried out for the samples calcined at 1100 °C, due to its performing both structural and quantitative data. Concerning the samples synthesised at lower temperatures, the rutile-to-anatase ratio was measured through the Spurr-Myers procedure [24] and the estimate of accessory phases was accomplished by the RIR method, due to the faster elaboration time of these methods without compromising the accuracy of the results.

3. Results and discussion

3.1. Anatase-to-rutile transition

This polymorphic reaction is heavily affected by the presence of dopants, as it can be seen in Figs. 1 and 2, that contributes to lower the onset temperature of the A → R transformation down to 300 °C with respect to the undoped titania, though the transition rate appears to be more or less the same in most samples.

However, there are clear differences among the several chromophores (Fig. 2) and counterions (Fig. 3) which should play a different role: ions with valence (II) or (III) such as chromophores, are expected to diffuse in the titania lattice, increasing the oxygen vacancy concentration, that is the main mechanism promoting the A → R transformation [8–9,25–26]. In contrast, elements with valence ≥(IV), such as

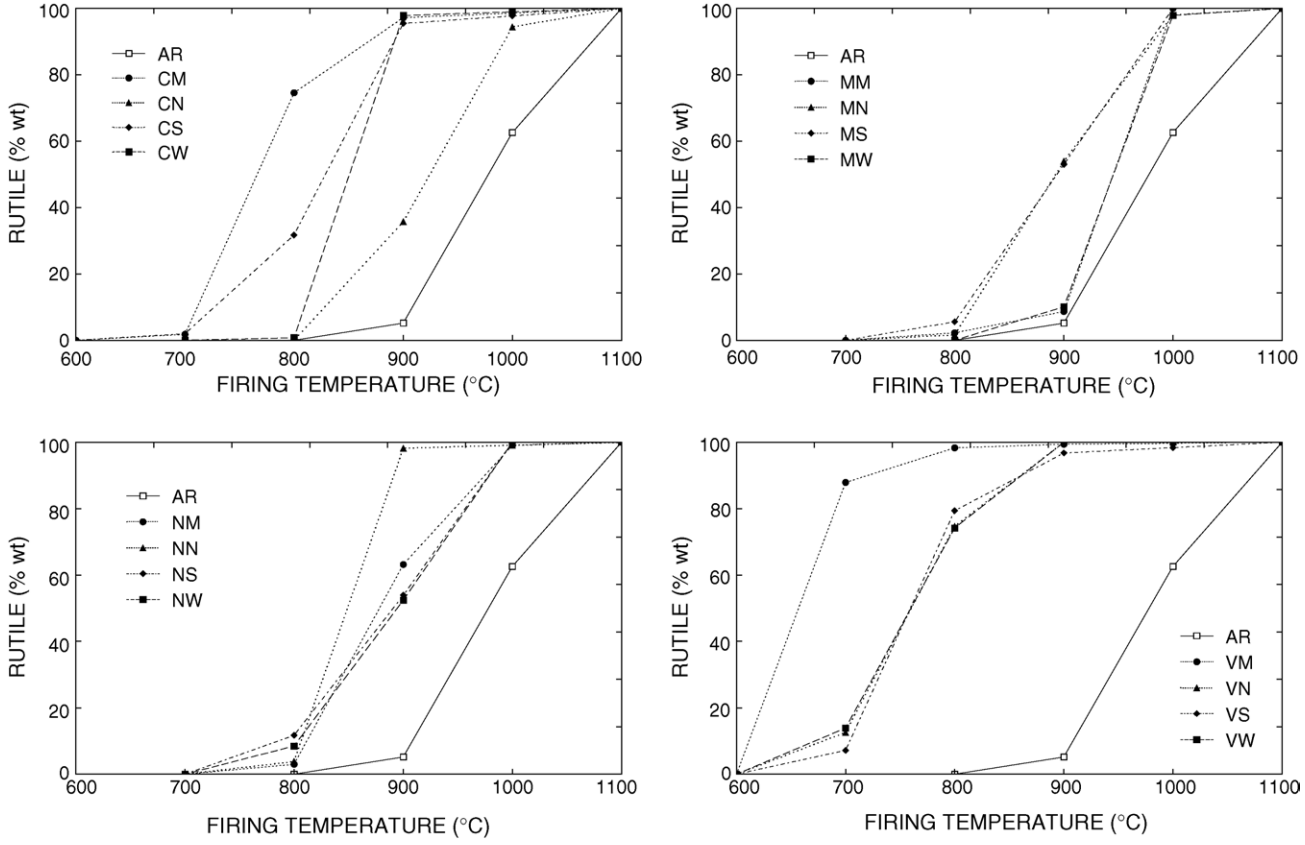

Fig. 2. Effect of chromophores (Cr, Mn, Ni, V) on the anatase-to-rutile transformation at various firing temperatures.

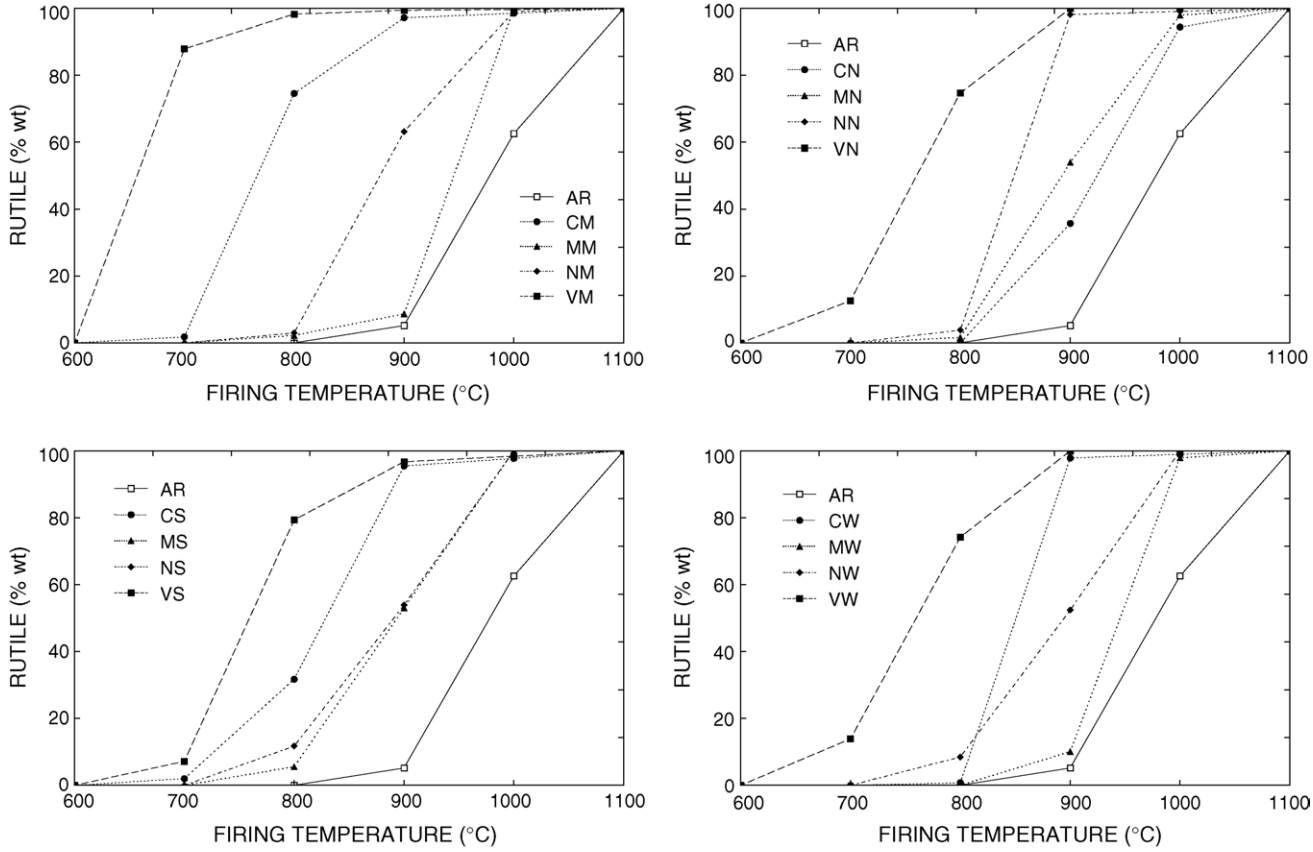

Fig. 3. Effect of chromophores (Mo, Nb, Sb, W) on the anatase-to-rutile transformation at various firing temperatures.

counterions, should inhibit the polymorphic reaction, basically through a charge balance of the rutile structure [7–10,14].

The most effective element is vanadium, that provokes a drop of the A → R onset temperature as low as 200 °C (when co-doped with Nb, Sb or W) or even almost 300 °C, when associated with Mo.

Chromium exhibits a noticeable effect on the A → R conversion, though influenced by the occurrence of counterions, which brings about a temperature decrease between 50 and 200 °C in respect of pure TiO_2, in the following order: Nb > W > Sb > Mo.

The decrease of the temperature of A → R transformation is the same (∼100 °C) in all the Ni-doped pigments; just the sample NN seems to show a faster kinetics, suggested by the steeper slope of the cumulative curve of the rutile amount in Fig. 2.

As far as manganese is concerned, a lowered onset temperature was found only for the systems containing Nb or Sb (−100 °C) while the samples coupling Mn + W or Mn + Mo began the titania polymorphic reaction more or less at the same temperature as undoped TiO_2, though a faster rate of rutile formation appeared.

The effect of counterions is almost entirely hidden by the prevailing role of chromophores (Fig. 3). In every case, the onset temperature of A → R transformation seems to follow the order: V < Cr < Ni < Mn, the only exception being the coupling Cr + Nb, which exhibits a shift downward of just ∼50 °C.

This circumstance suggests that the temperature of A → R transition is also affected by secondary phases, which essentially delay the diffusion of chromophores in the titania lattice, even if they could play as a nucleation point for rutile [7–8]. As a matter of fact, the samples with the higher A → R onset temperature (i.e. CN, MM and MW) are those containing significant amounts of accessory phases, such as $CrNbO_4$, $MnMoO_4$ or $MnWO_4$.

3.2. Occurrence of accessory phases

During the synthesis of rutile pigments, complex solid state reactions occur among the phases containing chromophores and counterions, which lead to the progressive decomposition of precursors and to the formation of transitory phases, often represented by double oxides of chromophores + counterions (e.g. $CrNbO_4$ or $MnWO_4$). These reactions take place essentially in the 700–1000 °C range, as below these temperatures the precursors are still to a large extent stable, while after calcination at 1100 °C almost uniquely rutile is present.

Among the Cr-bearing pigments, the CN system is clearly differing because the transitory phase $CrNbO_4$ is rather stable by the thermal point of view, persisting well over 1000 °C (Fig. 4). The other systems, on the contrary, develop

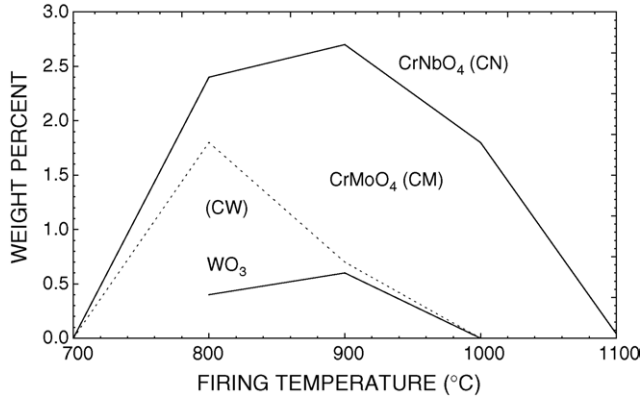

Fig. 4. Transitory phases formed during the synthesis of Cr-bearing rutile pigments co-doped with Mo (CM), Nb (CN) or W (CW).

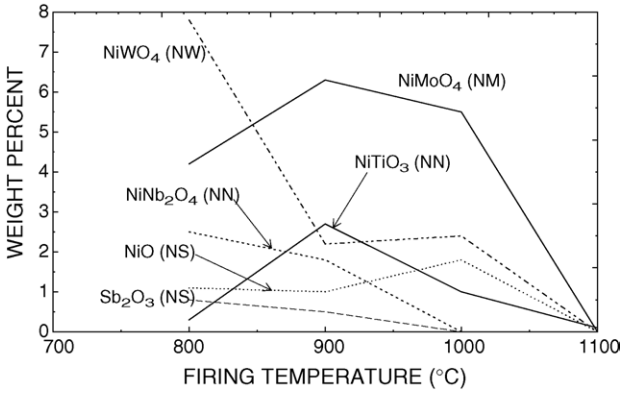

Fig. 6. Transitory phases formed during the synthesis of Ni-bearing rutile pigments co-doped with Mo (NM), Nb (NN), Sb (NS) or W (NW).

only traces of $CrMoO_4$ (CM) or just a modest excess of WO_3 (CW) that, however, are completely reacted after firing at 1000 °C. In the case of the CS system, no secondary phases were found in significant amounts, so that the trend $Sb_2O_3 \rightarrow Sb_2O_4 \rightarrow Sb_2O_5$ – prior to any antimony incorporation in the titania lattice [3] – was not appreciable.

In the Mn-doped samples, the decomposition of Mn_2O_3 is accomplished between 700 and 1000 °C with formation of $MnNb_2O_6$, $MnSb_2O_6$, $MnMoO_4$ or Mn_2TiO_4 (Fig. 5). All these double oxides contain manganese in the form (II), confirming the observations that foreign ions do change valence in the meanwhile of the A → R transformation [3,8]. Some of these phases are particularly stable, being found in significant amounts even after calcining at 1100 °C ($MnMoO_4$ and $MnWO_4$).

Several secondary phases were found after the synthesis of Ni-bearing pigments, in which the nickel is always attributable to the valence (II). Nickel molibdate and nickel wolframate are formed in the NM and NW samples, respectively, and persist up to over 1000 °C (Fig. 6). In the NN system, $NiNb_2O_6$ and $NiTiO_3$ are formed contemporarily to the A → R transition and both disappear only after firing at 1100 °C. Just some traces of precursors (Sb_2O_3 and NiO) are detectable in the NS pigments and they are totally reacted at 1100 °C. These trends for the Ti–Sb–Ni and Ti–Nb–Ni systems are considerably different in respect of literature data [3,18] maybe because of differences in chromophore and counterions loading as well as firing conditions, that, as well known, are two of the main factors influencing solid state reactions.

Transitory phases are less abundant in the V-bearing pigments: the VN system does not develop any secondary compound, while in the other samples traces of V_2O_3 and $SbVO_4$ (VS) or $VMoO_4$ (VM) are found. The VW pigment is characterised by a fair amount of WO_3 and the occurrence of a Ti^{3+}/Ti^{4+} oxide (Ti_5O_9) over 1000 °C (Fig. 7).

3.3. Rutile crystal structure

The structural data achieved by Rietveld refinements of the pigments synthesised at 1100 °C are summarised in Tables 1 and 2.

By contrasting the cell parameters, the points may be grouped in four series, each one referred to a certain counterion, that seem to be ordered according to an increasing c value: W ∼ Mo < Nb < Sb, with the single exception of the NM pigment (Fig. 8). This trend could be explained by a progressive increase of ionic radii, assuming

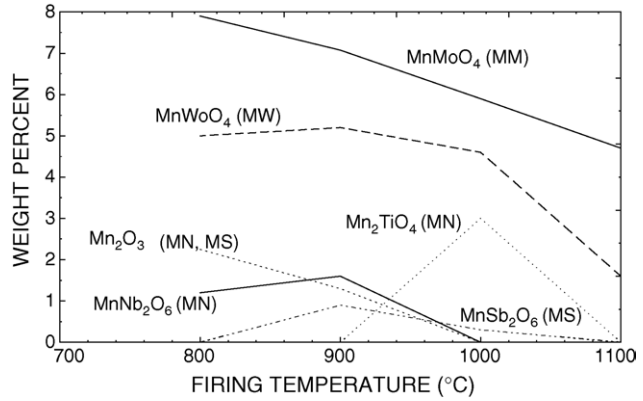

Fig. 5. Transitory phases formed during the synthesis of Mn-bearing rutile pigments co-doped with Mo (MM), Nb (MN), Sb (MS) or W (MW).

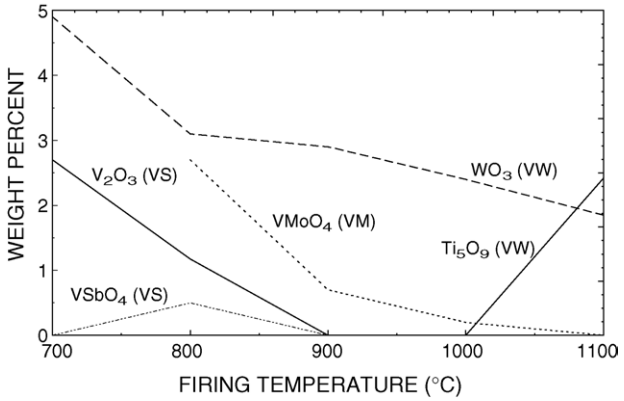

Fig. 7. Transitory phases formed during the synthesis of V-bearing rutile pigments co-doped with Mo (VM), Sb (VS) or W (VW).

Table 2
Ti–O bond lengths and degree of distortion of TiO_6 octahedron (BLD = bond length distortion) calculated by Rieveld refinements of X-ray diffraction patterns of rutile pigments synthesised at 1100 °C

Sample	Ti–O bond length (Å)			Distortion of TiO_6 octahedron (BLD)
	Apical distance (2×)	Basal distance (4×)	Average distance (6×)	
AA	1.979 (1)	1.950 (1)	1.960	0.145
CM	1.971 (1)	1.955 (2)	1.960	0.117
CN	1.975 (2)	1.955 (2)	1.961	0.135
CS	1.982 (1)	1.950 (1)	1.961	0.158
CW	1.967 (1)	1.957 (1)	1.960	0.091
MM	1.975 (1)	1.953 (2)	1.960	0.152
MN	1.983 (2)	1.949 (2)	1.960	0.206
MS	1.969 (1)	1.958 (2)	1.961	0.102
MW	1.980 (1)	1.951 (1)	1.960	0.149
NM	1.975 (1)	1.952 (2)	1.960	0.154
NN	1.976 (1)	1.954 (1)	1.962	0.108
NS	1.975 (2)	1.955 (1)	1.962	0.100
NW	1.970 (2)	1.957 (2)	1.961	0.104
VM	1.968 (1)	1.954 (2)	1.958	0.123
VN	1.972 (1)	1.954 (1)	1.960	0.092
VS	1.972 (1)	1.955 (1)	1.961	0.083
VW	1.957 (1)	1.963 (1)	1.961	0.029

Note: values shown in parentheses are estimated standard deviations in the last place. BLD: bond length distortion = $100/6 \times \Sigma_i|(M–O)_i – \langle M–O\rangle|/\langle M–O\rangle$ [27].

the following prevalent valences: W^{5+} (62 pm) ~ Mo^{5+} (62 pm) < Nb^{5+} (64 pm) < $Sb^{3+,5+}$ (mean 68 pm). In this hypothesis, antimony is incorporated into the rutile structure with both (III) and (V) valences (ionic radii 76 and 60 pm, respectively). On the one side, Sb^{5+} should be easily camoufled, having the same ionic radius of Ti^{4+} (60.5 pm); on the other side, the occurrence of Sb^{3+} seems to be necessary to account for the elongation of *c* axis; moreover, its presence in rutile pigments is claimed in the literature [6,13]. However, it might be reasonably supposed that the Sb^{3+}/Sb^{5+} ratio varies in order to balance the lattice charge, as required by the valence of the chromophore ion. Similarly, both molybdenum and tungsten may occur in the (V) or (VI) forms, which have close values of ionic radii, depending on the chromophore valence, as suggested by Maloney [3].

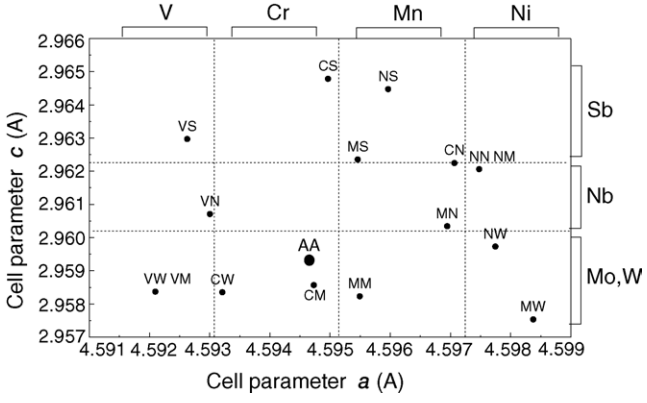

Fig. 8. Cell parameters *a* vs. *c* of rutile pigments synthesised at 1100 °C.

As far as the parameter *a* is concerned, a trend linked to the ionic size of chromophores can be appreciated: V < Cr < Mn ≤ Ni. This ranking is evident in the series co-doped with Mo or Sb, even if the order is Ni < Mn in the W-doped samples and a value larger than expected was found for the CN system (Fig. 8). The overall tendency might be justified by assuming the following ionic radii: V^{4+} (58 pm) < Cr^{3+} (62 pm) < Mn^{3+} (65 pm) < Ni^{2+} (69 pm). However, this hypothesis is not in full agreement with the above-discussed anatase-to-rutile transformation, for which the larger the valence gap between chromophore and Ti^{4+}, the lower the onset temperature, due to an increase of the oxygen vacancy concentration [9,24].

All the changes of cell parameters in the Cr- and Ni-doped rutile are in good agreement with the literature data [3,18,20] but for the Ti–Mn–Sb system, which does not exhibit the same strong structure enlargement as in the Maloney's sample [3].

As a matter of fact, the variations in rutile lattice could also be affected by non-stoichiometry due to an oxygen vacancy mechanism acting for charge compensation. In this standview, the valence (IV) is not able to explain the efficiency of vanadium to reduce the A → R transition temperature as low as 200–300 °C; hence, the occurrence of V^{3+} should be claimed, if other phenomena are not involved, such as a particularly efficient diffusion of V into the rutile lattice [11]. In the case of Ni-doped pigments, the valence (II) should promote a more pronounced lowering of the A → R temperature, being the difference as low as 100 °C with the undoped rutile. Furthermore, the ionic radius of Ni^{2+} (69 pm) is significantly larger than that of Ti^{4+} (60.5 pm), while the size of Ni^{3+} (60 pm) would fit much better the size of the Ti in octahedral coordination.

The cell volume of rutile exhibits a certain positive correlation with a weighed ionic radius, calculated by the octahedral site occupancy (Ti^{4+}, chromophores, counterions) once the following prevailing valence of dopants is supposed: Cr^{3+}, Mn^{3+}, Ni^{2+}/Ni^{3+}, V^{4+}, Mo^{5+}/Mo^{6+}, Nb^{5+}, Sb^{5+}/Sb^{3+}, W^{5+}/W^{6+} (Fig. 9).

By increasing the cell parameter *a*, a vague tendency to increase the distortion of the octahedral site (BLD) arose. In

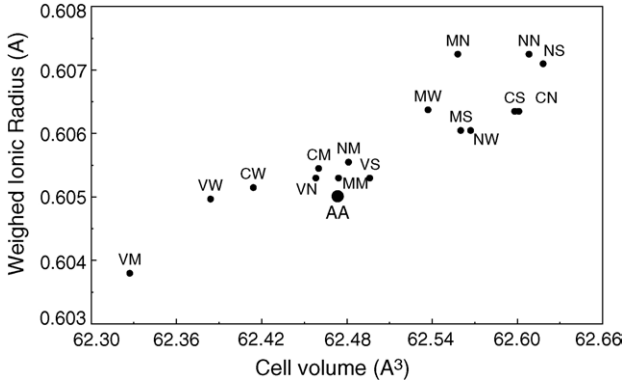

Fig. 9. Rutile cell volume vs. weighed ionic radius calculated by titanium, chromophore and counterion occupancy of octahedral site.

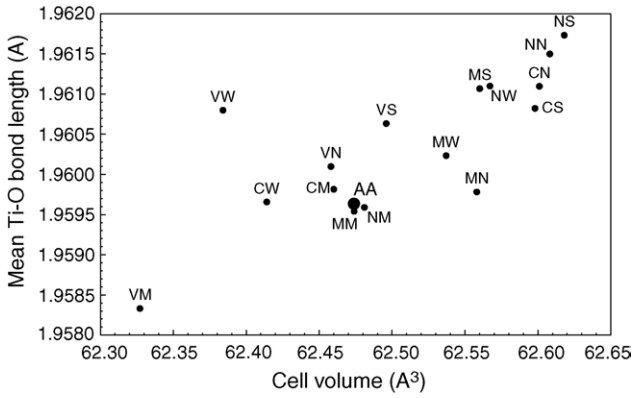

Fig. 10. Rutile cell volume vs. mean Ti–O bond length in the octahedral site.

reality, this trend could be traced in the samples doped with Cr, Mn or V, because the Ni-series exhibits similar BLDs against variable values of *a*.

A good positive correlation exists between the cell volume and the averaged Ti–O bond length; there is the exception of the sample VW, which shows a mean Ti–O distance clearly larger than expected on the basis of its cell volume (Fig. 10).

Contrasting the apical Ti–O distance with the mean basal Ti–O distance of TiO_6 octahedron, a common trend demonstrates that the co-doping with chromophore plus counterion implies a decrease of the apical elongation and an enlargement of the equatorial plane of the octahedron, with respect to the undoped rutile (AA). At all events, some pigments exhibit just modest changes of the Ti–O distances (i.e. CS, MM, MW, NM) while the MN system presents an opposite trend, having shorter basal distances and a larger apical distance than the reference rutile structure. In the pigment VW, the TiO_6 octahedron appears to be flattenened with basal distances longer than the apical ones.

4. Conclusion

Several solid state reactions occur during the synthesis of rutile pigments, involving both the anatase-to-rutile transformation and the formation of transitory phases, mostly double oxides of chromophore + counterion. The A → R transition is strongly affected by the presence of chromophore elements; a clear lowering of the onset temperature was found and the order is: V < Cr < Ni < Mn. The effect of counterions is almost totally masked by that of chromophores; however, in the Cr-doped series the A → R temperature is lowered according to the sequence: Mo < Sb < W < Nb, that well corresponds to the inhibiting role of each counterion described in the literature. The higher onset temperatures of the A → R polymorphic reaction were registered when particularly stable accessory compounds occurred, e.g. $CrNbO_4$, $MnMoO_4$, $MnWO_4$.

The transitory phases are basically developed between 700 and 1000 °C, being chromophores and counterions fully diffused in the rutile lattice after firing at 1100 °C (except for Ti–Mn–Mo, Ti–Mn–W and Ti–V–W systems). These secondary compounds are abundant in the Mn- and Ni-doped systems, while appear to be scarce in Cr- and V-bearing pigments. The stoichiometry of these phases suggests the presence of a unique valence for Cr^{3+}, Nb^{5+}, Ni^{2+} and W^{6+}, while mixed valences are implied for Mn (II–III), Mo (V–VI), Sb (III–V) and V (III–IV).

Chromophores and counterions modify in a complex way the crystal structure of rutile pigments:

- the cell parameter *c* appears to be mainly affected by counterions, being increased along the series: W ∼ Mo < Nb < Sb;
- the cell parameter *a* is principally influenced by chromophores, being increased according to the sequence: V < Cr < Mn < Ni;
- the cell volume is positively correlated with the weighed ionic radius in the octahedral site, assuming the following prevalent valence of cations: Cr^{3+}, Mn^{3+}, Ni^{2+}/Ni^{3+}, V^{4+}, Mo^{5+}, Nb^{5+}, Sb^{5+}/Sb^{3+}, W^{5+};
- the increment of the parameter *a* implies a progressive distortion of the octahedral site;
- the increasing cell volume brings about a gradual elongation of the averaged Ti–O bond length;
- the doping with chromophores and counterions causes in most cases a flattening of the TiO_6 octahedron, with longer equatorial Ti–O distances and a shorter apical Ti–O distance;
- the pigment VW is clearly distinguished from the others for its minimum Ti–O bond length distortion, an almost regular TiO_6 octahedron, and the occurrence of Ti^{3+} within the accessory compound Ti_5O_9.

However, some chromophore valences supposed are unusual (e.g. Ni^{3+}) and/or not in full agreement with the expected effect on the A → R transformation (i.e. Ni^{2+} and V^{4+}). It is likely that non-stoichiometry might play a significant role on structural variations, being oxygen vacancy a possible alternative mechanism of charge balance in the rutile lattice.

References

[1] Italian Ceramic Society, Colour, Pigments and Colouring in Ceramics, SALA, Modena, 2003, pp. 1–295.
[2] P.E. Lòpez, J.B. Carda Castellò, C.E. Cordoncillo, Esmaltes y pigmentos ceràmicos, Faenza Editrice Iberica, 2001, pp. 1–300.
[3] J. Maloney, Titanate pigments: colored rutile, priderite, and pseudobrookite structured pigments, in: H.M. Smith (Ed.), High Performance Pigments, Wiley-VCH, 2002, pp. 53–73.
[4] F. Hund, Mixed-phase pigments with rutile structures, Angew. Chem. Int. 1 (1) (1962) 41–45.
[5] DCMA, Classification and Chemical Description of the Complex Inorganic Color Pigments, third ed., 'Dry Color Manufacturers' Association, Alexandria, VA, 1991.

[6] R.A. Eppler, Effect of antimony oxide on the anatase-rutile transformation in titanium dioxide, J. Am. Ceram. Soc. 70 (4) (1987) C64–C66.
[7] R.A. Eppler, Niobium and tungstenum oxides in titania-opacified porcelain enamels, J. Am. Ceram. Soc. 52 (12) (1973) 879–881.
[8] K.J.D. MacKenzie, The calcination of titania. Part IV: The effect of additives on the anatase-rutile transformation, Trans. J. Br. Ceram. Soc. 74 (1975) 29–34.
[9] K.J.D. MacKenzie, The calcination of titania. Part V: Kinetics and mechanism of the anatase-rutile transformation in the presence of additives, Trans. J. Br. Ceram. Soc. 74 (1975) 77–84.
[10] C. Cristiani, M. Bellotto, P. Forzatti, F. Bregani, On the morphological properties of tungsta-titania de-noxing catalysts, J. Mater. Res. 8 (8) (1993) 2019–2025.
[11] P. Lostak, Z. Cernosek, E. Cernoskova, L. Benes, J. Kroutil, V. Rambousek, Real structure of TiO_2 in samples of the TiO_2–V_2O_5 system, J. Mater. Sci. 28 (5) (1993) 1189–1193.
[12] B.M. Reddy, E.P. Reddy, S. Mehdi, Phase transformation study of titania in V_2O_5/TiO_2 and MoO_3/TiO_2 catalysts by X-ray diffraction analysis, Mater. Chem. Phys. 36 (3–4) (1994) 276–281.
[13] G. Croft, M.J. Fuller, Crystalline oxidic solid solutions of tin (IV) and titanium (IV), their coloration by and thermal reaction with some metal ions. Part 1: The rutile $Sn_xTi_{(1-x)}O_2$ system and its interaction with V (V), Cr (III), Cr (IV), Mn (II), Fe (III), Co (II), Ni (II), Cu (II) and Sb (III), Br. Ceram. Trans. 78 (3) (1979) 52–56.
[14] L.E. Depero, L. Sangaletti, B. Allieri, E. Bontempi, R. Salari, M. Zocchi, C. Casale, M. Notaro, Niobium–titanium oxide powders obtained by laser-induced synthesis: microstructure and structure evolution from diffraction data, J. Mater. Res. 13 (6) (1998) 1644–1649.
[15] M.A. Tena, A. Mestre, A. García, S. Sorlí, G. Monrós, Synthesis of gray ceramic pigments with rutile structure from alkoxides, J. Sol–Gel Sci. Technol. 26 (2003) 813–816.
[16] H. Krause, H. Reamer, J. Martin, Mixed rutile crystal formation in the Ti–Ni–Sb–O system. Part I: Rutile solid solution and the reaction diagram, Mater. Res. Bull. 3 (1968) 233–240.
[17] H. Krause, Mixed rutile crystal formation in the Ti–Ni–Sb–O system. Part II: Mechanism of rutile solid solution, Mater. Res. Bull. 3 (1968) 241–252.
[18] S. Sorlí, M.A. Tena, J.A. Badenes, J. Calbo, M. Llusar, G. Monrós, Structure and color of $Ni_xA_{1-3x}B_{2x}O_2$ (A = Ti,Sn; B = Sb,Nb) solid solutions, J. Eur. Ceram. Soc. 24 (8) (2004) 2425–2432.
[19] M.A. Tena, M. Llusar, J.A. Badenes, J. Calbo, G. Monrós, Structural and electrical conductivity studies on (M,V)-TiO_2 (M = Al, Cr, Fe) rutile solid solutions at high temperature, J. Mater. Sci. Mater. Electr. 15 (4) (2004) 265–270.
[20] M.A. Tena, P. Escribano, G. Monrós, J. Carda, J. Alarcón, Influence of niobate structures on the formation of rutile solid solutions [$M^{III}NbO_4TiO_2$, where M^{III} = Al, Fe, Cr], Mater. Res. Bull. 27 (1992) 1301–1308.
[21] A.C. Larson, R.B. Von Dreele, General Structure Analysis System (GSAS), Los Alamos National Laboratory Report LAUR, 2000, pp. 86–748.
[22] B.H. Toby, EXPGUI, a graphical user interface for GSAS, J. Appl. Cryst. 34 (2001) 210–221.
[23] C.J. Howard, T.M. Sabine, F. Dickson, Structural and thermal parameters for rutile and anatase, Acta Cryst. B47 (1991) 462–468.
[24] R.A. Spurr, H. Myers, Quantitative analysis of anatase–rutile mixtures with an X-ray diffractometer, Anal. Chem. 29 (5) (1957) 760–762.
[25] P.I. Gouma, M.J. Mills, Anatase-to-rutile transformation in titania powders, J. Am. Ceram. Soc. 84 (3) (2001) 619–622.
[26] H. Zhang, J.F. Banfield, Phase transformation of nanocrystalline anatase-to-rutile via combined interface and surface nucleation, J. Mater. Res. 15 (2) (2000) 437–448.
[27] B. Renner, G. Lehmann, Correlation of angular and bond length distortions in TO_4 units in crystals, Zeit. Krist. 175 (1986) 43–59.